Monte-Carlo Based Comparison of the Personal Dose for Emplacement Scenarios of Spent Nuclear Fuel Casks in Generic Deep Geological Repositories

Héctor Saurí Suárez, Bo Pang, Frank Becker and Volker Metz

Best Paper Award

The paper "Monte-Carlo Based Comparison of the Personal Dose for Emplacement Scenarios of Spent Nuclear Fuel Casks in Generic Deep Geological Repositories" by Héctor Saurí Suárez, Bo Pang, Frank Becker and Volker Metz has been awarded as Best Paper of the 48th Annual Meeting on Nuclear Technology (AMNT 2017), Berlin, 16 and 17 May 2017.

1 Introduction

When a high-level nuclear waste cask is transported to its final position in a deep geological disposal facility, the radiation exposure received by the workers in such a facility is expected to be significantly influenced by the materials of the surrounding layers. Moreover, the question arises if there is an enhanced directional dependent influence on the personal radiation exposure in such facilities since certain amount of backscattered radiation comes from the back and lateral sides. Hence, it is of interest to study the influence of the worker's position and its orientation on the personal dose assessment.

In the current study, the general-purpose Monte-Carlo N-Particle code MCNP6 *[Pelowitz et al., 2013]* was employed to calculate the radiation field around POLLUX® type shielding casks *[Janberg and Spilker, 1998; Filbert et al., 2011]* loaded with spent nuclear fuel (SNF), which were emplaced in horizontal drifts of deep geological repositories. Furthermore, a simplified mathematical phantom was used to represent a worker inside the facility, in order to calculate the personal radiation exposure for working scenarios with MCNP6. Emplacement in two different geological disposal facilities was considered, i.e. a horizontal drift in rock salt (from now on in short as "rock salt drift" or RSD) and a horizontal drift in a clay or shale formation (from now on in short as "clay drift" or CLD). In contrast to a repository in rock salt, drifts and access galleries of a repository in soft rock, such as clay and shale, have to be reinforced with concrete lining with a thickness of several decimetres *[e.g. Chen et al., 2014; Leon Vargas et al., 2017]*. The radiation field was calculated in terms of ambient dose equivalent for both drifts at different positions to the shielding cask, which is disposed on the ground of the drift. In order to study the dependence of the worker's orientation towards the cask on the personal exposure, simulations with different angles between phantom and POLLUX® cask were performed in RSD. Finally, a comparison between the calculated personal dose rate during a working scenario in RSD and in CLD was conducted.

2 Methodology

2.1 Waste inventories considered for POLLUX® type casks

Based on the average inventory of used fuel elements discharged from pressurized water reactors (PWR) in Germany *[Peiffer et al. 2011]*, a representative waste loading of 90 % uranium oxide (UOX) fuel and 10 % mixed-oxide (MOX) fuel with a burn-up of 55 GWd/t(HM) was considered. The POLLUX® self-shielding cask *[Janberg and Spilker, 1998; Filbert et al., 2011]*, designed for deep geological disposal in RSD, was employed for both RSD and CLD. In our model for disposal in RSD, a POLLUX® cask, loaded with fuel rods of ten PWR fuel assemblies was numerically simulated. This corresponds to a waste load of about 5.45 metric tons heavy metal *(tHM)*. The cask with fuel rods of one MOX and nine UOX fuel assemblies is herein after referred to as POLLUX-10. Due to temperature restrictions regarding emplacement of casks with heat-generating waste in clay and shale formations *[Leon Vargas et al, 2017]*, for the emplacement in a CLD the maximum amount of fuel assemblies per cask was set to three. Therefore, one POLLUX® type cask with an homogeneous mixture of two thirds PWR-UOX and one third PWR-MOX fuel corresponding to one MOX and two UOX fuel assemblies, comprising 1.64 *tHM* (herein after referred to as POLLUX-3M), and two POLLUX® casks with an homogeneous mixture of PWR-UOX corresponding to three UOX fuel assemblies, comprising 1.64 *tHM* (herein after referred to as POLLUX-3U), were employed for the emplacement in a CLD. In general, the MOX fuel rods are supposed to be placed in the center of the cask surrounded by the UOX fuel rods. This arrangement provides an additional shielding for neutrons coming from MOX fuel rods. Hence, a homogeneous mixture will give conservative results since the MOX fuel is homogeneously distributed and supposed to be less shielded. Two zones were defined in a fuel rod, i.e. an "active zone" which contains the fuel pellets and an "inactive zone" which corresponds to the top and bottom of the fuel rod and it is mainly composed of Zircaloy cladding *[Janberg and Spilker, 1998]*. The effective density in these zones was calculated according to the equation:

$$\rho_{zone} = \frac{m_{zone}}{V_{canisterzone}}$$

where m_{zone} is the mass of the corresponding zone and $V_{canisterzone}$ is the total volume available in the POLLUX® type cask for that zone.

An average burnup of 55 gigawatt-days per metric ton of heavy metal *(GWd/tHM)* was assumed for both UOX and MOX SNF. Before emplacement a cooling time of the SNF was assumed to be 50 years after discharge from the reactor core. This duration corresponds to an assumed interim storage time before disposal of SNF in a deep geological disposal facility to be built in 2050 according to *BMUB [2015]*. Isotope mass of the SNF in dependence of the cooling time was taken from *[Peiffer et al., 2011]*. The SNF inventory is composed of hundreds of different isotopes, but many of them have negligibly small activities. As investigated in a previous study *[Pang et al., 2016]*, for the waste inventory

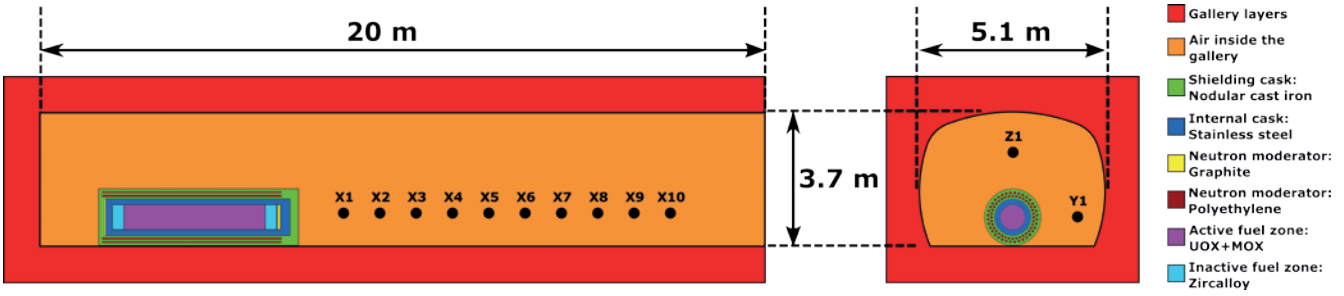

Fig. 1.
MCNP6 model of the emplacement drift with a POLLUX® cask loaded with irradiated UOX and MOX fuel. Black dots represent the position of the F5 tallies, where the letter indicates the axis direction and the number the distance in meters to the cask surface.

considered in this study, neutrons dominate the radiation field and exposure outside the shielding cask. Hence, only those isotopes that contribute significantly to neutron activity were considered when defining the radiation sources for simulations with MCNP6.

For the considered fuel inventory the main contributor to neutron emissions is the spontaneous fission of ^{244}Cm (90 % of the total emission) and ^{246}Cm (5 % of the total emission), while the contribution due to (α,n) reactions, mainly stemming from interactions with ^{18}O, is less than 5 %. The total neutron source strength for the POLLUX-10 inventory is $1.66 \cdot 10^{+9}$ neutrons/sec (n/s), while those for the POLLUX-3M and POLLUX-3U inventory are $9.02 \cdot 10^{+8}$ n/s and $3.24 \cdot 10^{+8}$ n/s, respectively.

2.2 Calculation of the ambient dose equivalent rate $\dot{H}^*(10)$

In the generic model for a repository for heat generating waste of *Stahlmann et al. [2015]*, an emplacement drift has a length of 57 m (RSD) and 63 m (CLD), respectively. The drift is surrounded by a host rock layer of at least 100 m thickness and several decimetres of concrete lining in the case of CLD. To simplify the calculations, the thickness of the drift walls, i.e. rock salt for POLLUX-10 and concrete lining for POLLUX-3M and POLLUX-3U, was set to 1 m in the MCNP6 model, which is sufficient to account for possible interactions of the radiation with the drift wall materials. With respect to interactions of neutrons and photons with clay and concrete, both materials are characterized by similar densities and elemental / oxidic compositions, dominated by SiO_2, CaO, Al_2O_3 and H_2O. **Figure 1** shows the modelling of the deep geological disposal facility and the POLLUX® type cask with MCNP6. As a simplification, only one cask (cylindrical form with a length of 5.5 m and an outer diameter of 1.56 m) was placed on the ground of the drift with its bottom surface at 2.63 m distance to the drift end side. Detailed geometrical information of POLLUX® type cask and the generic emplacement drifts can be found in *[Jaberg and Spilker, 1998; Filbert et al., 2011]* and *[Stahlmann et al., 2015]*, while the respective detailed MCNP6 models were already described in *[Pang et al., 2016]*, hence they are not shown here. Since the radiation scattered by the drift layers might have an important impact on the radiation field, a third drift was also modelled. This one has the same geometry as the ones described above but the surrounding wall layers were replaced by air, representing a cask free in air (from now on in short as FIA).

As denoted by black dots in **Fig. 1**, twelve MCNP6 point detector F5 tallies *[Pelowitz et al., 2013]* were employed to calculate the neutron fluence rate and the ambient dose equivalent rate $\dot{H}^*(10)$ at different positions inside the drift. Tallies X1, Y1 and Z1 (see **Fig. 1**) were defined to compare $\dot{H}^*(10)$ at 1 m distance to the cask surface in the respective directions. To study the change of $\dot{H}^*(10)$ with the distance to the cask, the tallies X1 to X10 (see **Fig. 1**) were also employed. The neutron fluence-to-ambient-dose-equivalent conversion coefficients given by *ICRP [1996]* were employed to convert the F5 tally results into $\dot{H}^*(10)$. To assess the precision of the result, MCNP6 produces a wealth of information about a simulation, which is represented by ten statistical checks *[see Pelowitz et al. (2013)]*. To pass the ten statistical checks, $2 \cdot 10^{+7}$ particles were required per simulation.

2.3 Calculation of the personal dose equivalent rate $\dot{H}_p(d)$

To obtain the personal dose equivalent rate $\dot{H}_p(d)$, a worker inside the drift was represented in this study with a simplified anthropomorphic phantom. This phantom is a virtual representation of the BOMAB (BOttle MAnnikin ABsorber) phantom, which models the head, neck, chest, abdomen, thighs, calves, and arms with cylinders or elliptical cylinders. A detailed description of its components can be found in *[U.S. Department of Energy, 2016]*. **Figure 2** shows the MCNP6 model of the phantom used in the current study.

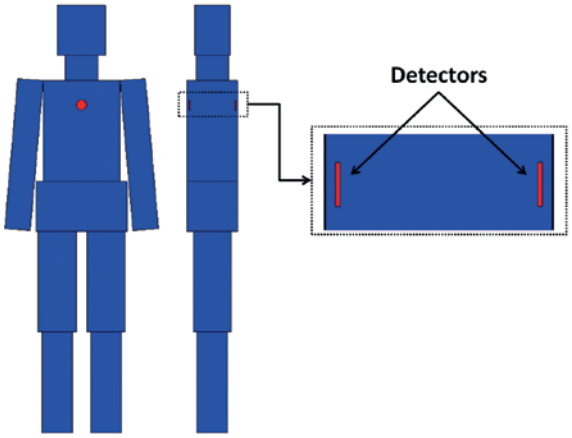

Fig. 2.
MCNP6 representation of the BOMAB phantom with a cylindrical detector at the front side (chest dosimeter) and at the back side (back dosimeter).

As recommended by *ICRP, [2007]* the personal dose equivalent rate $\dot{H}_p(d)$ at a depth d=10 mm gives a conservative assessment of the effective dose rate under most irradiation conditions. However, this requires the personal dosimeter to be worn at a position on the body which is representative with respect to the exposure. In general it is recommended to wear a dosimeter in front of the chest, where $\dot{H}_p(d)$ is supposed to give a conservative estimation of the effective dose even in cases of lateral or isotropic radiation incidence on the body *[ICRP, 2007]*. However, in cases of exposure from the back, the question arises if a dosimeter worn at the front still appropriately assesses the effective dose. For a worker inside an emplacement drift, as investigated in the current study, a certain amount of

radiation incidents on the backside due to the backscattered radiation by the surrounding drift layers. Therefore, in order to study the influence of the backscattered radiation, two cylindrical detectors (2 cm radius and 0.2 cm length) were modelled in the phantom (see **Fig. 2**): one on the front side (representing a dosimeter worn in front of the chest) and another one on the back side (representing a dosimeter worn at the back side), both at 10 mm depth to calculate $\dot{H}_p(d)$. The personal dose equivalent rate $\dot{H}_p(d)$ is calculated as:

$$\dot{H}_p(10) = \int_{E_{min}}^{E_{max}} \left(\dot{D}_n(E_n)Q_n(E_n) + \dot{D}_\gamma(E_\gamma)Q_\gamma(E_\gamma)\right) dE$$

Where $\dot{D}_n(E_n)$ is the neutron absorbed dose rate, and $\dot{D}_\gamma(E_\gamma)$ is the gamma absorbed dose rate. The quality factor for photons (Q_γ) is equal to 1; while for neutrons (Q_n) it is dependent on the neutron energy (E_n) and the linear energy transfer (L) according to:

$$Q_n(E_n) = \frac{1}{D}\int_{L_{\min}}^{L_{\max}} Q(L)D(L,E_n)dL$$

The MCNP6 energy deposition tally F6 *[Pelowitz et al., 2013]* was used to calculate the absorbed dose rate (D). Tabulated values for $Q_n(E_n)$ were taken from *[Siebert and Schuhmacher, 1995]* to convert the F6 tally results to dose equivalents.

To study the effect the orientation of the worker with respect to the shielding cask, five simulations with the phantom at angles of 0°, 15°, 45°, 60°, and 90° with respect to POLLUX-10 symmetrical axis (see **Figure 3**) were performed in RSD. For each simulation, the $\dot{H}_p(10)$ obtained with the front dosimeter and the sum of the $\dot{H}_p(10)$ obtained with the front and back dosimeter were compared to check if the use of only one dosimeter may underestimate the received dose rate. To reduce the calculation time, the MCNP6 variance reduction technique "geometry splitting" *[Pelowitz et al., 2013]* was applied. Using geometry splitting, a weighting is assigned in the following way: regions near the tallies (cylindrical detectors in the phantom) are assigned with a greater importance than regions farther away. When a particle leaves a region it is split/killed according to the importance ratio adjusting the weight of the remaining particles to leave the tally unbiased. A total of $1 \cdot 10^{+8}$ particles were required per simulation to pass the ten MCNP6 statistical checks.

2.4 Comparison of $\dot{H}_p(10)$ in the rock salt and clay formation drifts during a typical working scenario

The above explained methodology, i.e. the use of two dosimeters for the estimation of $\dot{H}_p(10)$ was applied to the working scenario of POLLUX® disposal in the emplacement drift based on the proposal of DBE TECHNOLOGY GmbH *[Filbert et al., 1995]*. **Figure 4** shows the MCNP6 models of four main working steps in the cask disposal procedure as well as the main components. A description of their geometry can be found in *[Bollinger-fehr et al., 2011]*. The four steps are: first the cask is transported on a carriage through the drift with an electric locomotive with a driver sitting inside the cabin (see **Fig. 4a**). Once it arrives at the disposal position, as shown in **Fig. 4b**, the cask is slowly positioned under a storage equipment which elevates the cask from the carriage to allow locomotive and carriage to drive back. Once the locomotive is driven back, the storage equipment places the cask on the ground (see **Fig. 4c**). Finally, as shown in **Fig. 4d**, the locomotive moves the storage equipment to the next disposal position.

Since the cask geometry of POLLUX-3M and POLLUX-3U are equal to that of POLLUX-10, the same steps as described in **Fig. 4** were simulated for the disposal of POLLUX-10, POLLUX-3M and POLLUX-3U cask. To compare the radiation exposure, the same or a similar amount of SNF should be disposed in both emplacement drifts, i.e. one POLLUX-10 cask in RSD containing fuel rods of one MOX and nine UOX fuel assemblies (5.45 *tHM*) and three casks in CLD (one POLLUX-3M and two POLLUX-3U, in total 4.92 *tHM*). As the working steps are the same for the disposal of POLLUX-10, POLLUX-3M and POLLUX-3U, $\dot{H}_p(10)$ was employed to compare the radiation exposure in the different working steps as described above.

The driver sitting inside the cabin was represented in this study by the phantom (see **Fig. 2**). Since the worker stays all the time inside the cabin and faces the shielding cask, the angle between phantom and cask is always 0°. However, the amount of backscattered radiation may be further increased due to the reflection by the cabin walls and backscattered neutrons from the drift walls. To perform the MCNP6 simulations, geometry splitting was employed in the drift and inside the locomotive cabin to reduce the number of transported particles. To pass the ten MCNP6 statistical checks, $4 \cdot 10^{+8}$ particles were required for simulation of the transport and location under the storage equipment. For the placement and retreat of the storage

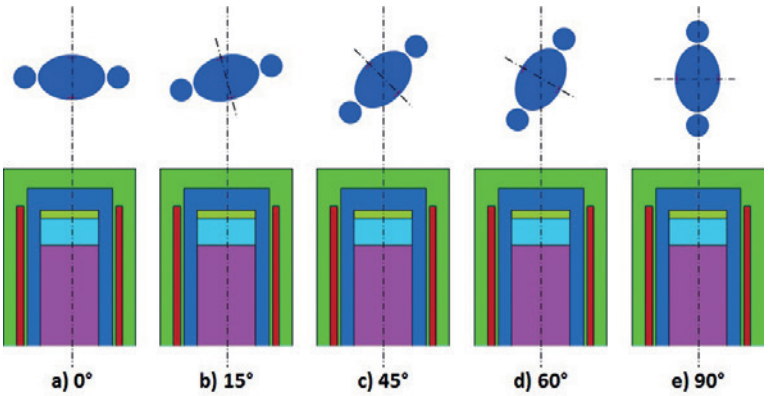

Fig. 3.
Different angles of the phantom with respect to POLLUX.

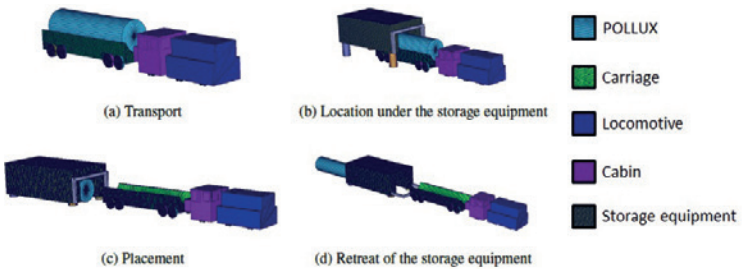

Fig. 4.
MCNP6 model of the four steps for a POLLUX® disposal scenario (for details see text).

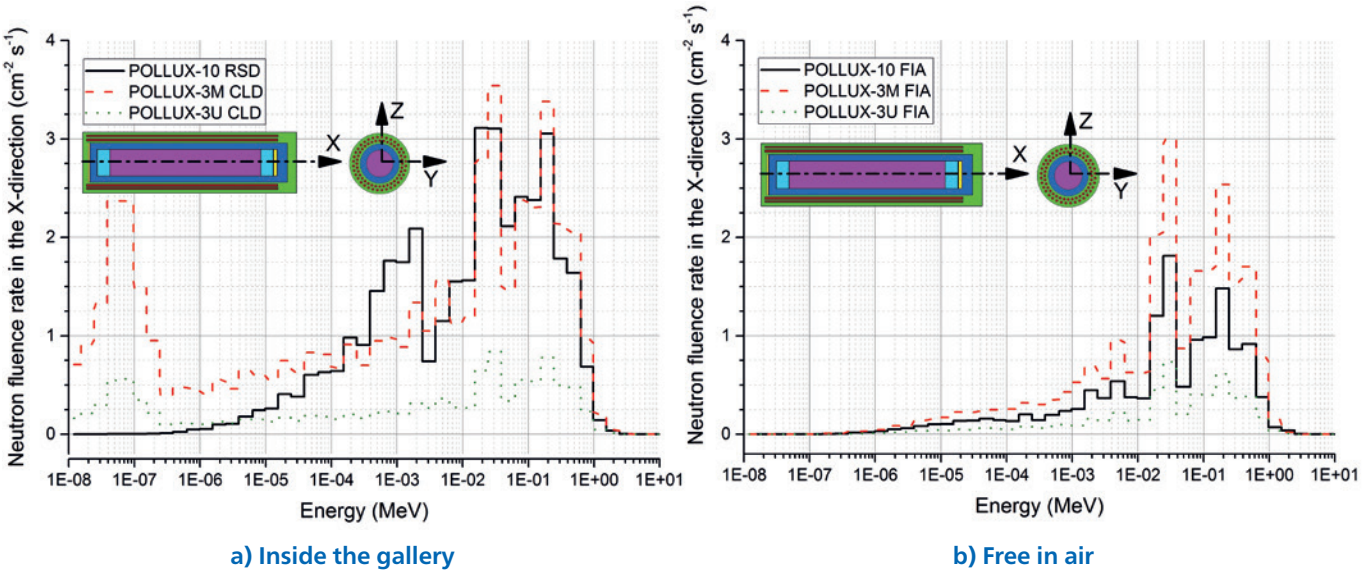

Fig. 5.
Spectral neutron fluence rate calculated with MCNP6 (for details see text).

equipment $1.5 \cdot 10^{+9}$ particles were required per simulation, since the distance between the cask and the phantom is larger.

3 Results and discussion

3.1 The ambient dose equivalent rate $\dot{H}^*(10)$ in the emplacement drift

Figure 5a and **Figure 5b** show the spectral fluence rate calculated with MCNP6 at 1 m distance to the cask surface in X direction inside the RSD and CLD as well as FIA. The relative error of the fluence rates in each energy bin is in general less than 4 %, except for some bins with fluence rates lower than 0.005 $cm^{-2}s^{-1}$. The effect of the backscattered radiation can be observed for the RSD with the local minimum of the spectral fluence rate between $2 \cdot 10^{-3}$ to $3 \cdot 10^{-3}$ MeV (**Fig. 5a**), which is caused by elastic neutron scattering on ^{23}Na (one of the main isotopes of the surrounding rock salt), which has a peak in the cross-section at $2.8 \cdot 10^{-3}$ MeV. In the CLD, the maximum between $1 \cdot 10^{-8}$ and $1 \cdot 10^{-6}$ MeV (**Fig. 5a**) shows the presence of moderated neutrons mainly due to interactions with ^{16}O content of the concrete lining (mainly composed of CaO, SiO_2, Al_2O_3, H_2O).

Figure 6 shows $\dot{H}^*(10)$ at 1 meter distance to cask surface in the different drifts as well as FIA. Since the cask shielding in the X direction is the thickest, $\dot{H}^*(10)$ outside the cask in the X direction is lower than that in Y and Z directions. For the FIA scenarios, $\dot{H}^*(10)$ in the X direction outside the POLLUX-10 cask is 24 % lower than that outside the POLLUX-3M, while in the Y and Z directions $\dot{H}^*(10)$ outside the POLLUX-10 cask is 24 % and 20 % higher than outside the POLLUX-3M, respectively. This can be explained due to the influence of the inactive zone at the top and bottom of the fuel rods (X direction).

Figure 7 shows the neutron spectra before and after the Zircaloy layer in the inactive zone for POLLUX-3M and POLLUX-10. The total neutron fluence rate before the inactive zone is higher for POLLUX-10 (1538 $cm^{-2}s^{-1}$) than for POLLUX-3M (861 $cm^{-2}s^{-1}$). According to the calculated density of the SNF (see Equation 1), which is for POLLUX-10 (active and inactive zone) 3 times larger than for POLLUX-3M, neutrons emitted in the X direction are stronger shielded by the Zircaloy layer in POLLUX-10 (total neutron fluence after the inactive zone 331 $cm^{-2}s^{-1}$) than in POLLUX-3M (total neutron fluence after the inactive zone 340 $cm^{-2}s^{-1}$).

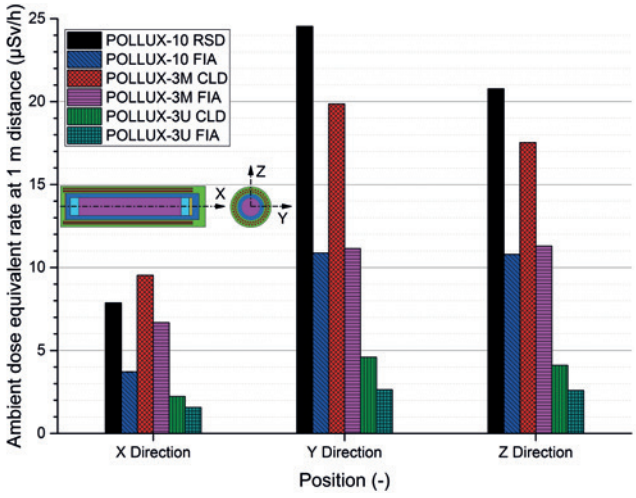

Fig. 6.
$\dot{H}^*(10)$ at 1 meter distance from the cask calculated with MCNP6 (for details see text).

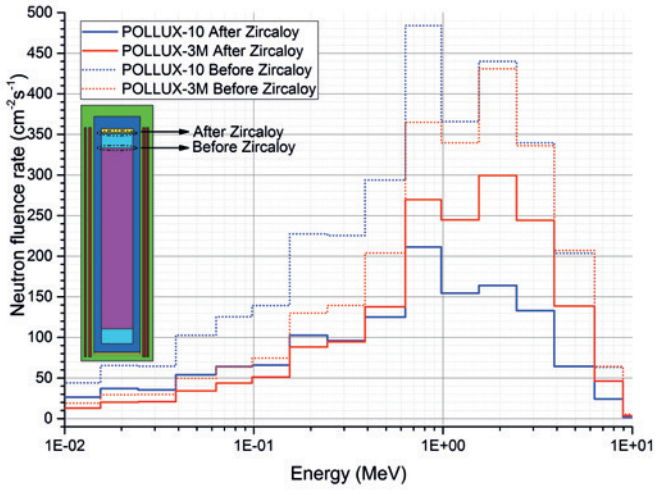

Fig. 7.
Spectral neutron fluence rate for the SNF calculated with MCNP6 (for details see text).

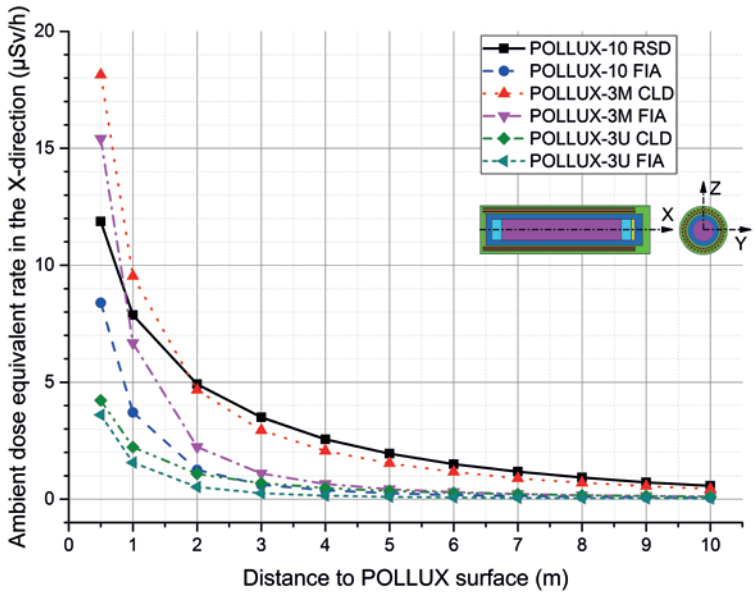

Fig. 8.
$\dot{H}^*(10)$ at different distances in the X direction for POLLUX-10 in rock salt, POLLUX-3M and POLLUX-3U in clay formation and POLLUX-3U in free air.

Figure 8 shows $\dot{H}^*(10)$ at different distances in the X direction for POLLUX-10, POLLUX-3M and POLLUX-3U as well as also for their respective FIA cases. $\dot{H}^*(10)$ for POLLUX-10 in RSD is between 30 % (at the cask surface) and 80 % (at 10 m distance) higher than for POLLUX-10 FIA. For POLLUX-3M and POLLUX-3U, $\dot{H}^*(10)$ in CLD is between 15 and 75 % higher than FIA. This reveals the important role of the backscattered radiation on the radiation field in a geological disposal facility. Figure 8 shows further that up to 1 m distance, $\dot{H}^*(10)$ is higher (up to 9 %) for POLLUX-3M in CLD than for POLLUX-10 in RSD. From this point on, the higher moderation of the concrete layers and the larger reflection of the salt layers lead to a higher $\dot{H}^*(10)$ in the RSD (between 10 % and 40 %). Since only spent UOX was loaded in a POLLUX-3U cask, $\dot{H}^*(10)$ for the case of POLLUX-3U is in general 63 % lower than that for POLLUX-3M.

3.2 Influence of the angle between phantom and disposal cask on $\dot{H}_p(10)$

Table 1 shows $\dot{H}_p(10)$ obtained with the detector at the chest $\dot{H}_p(10)_{Chest}$ and at the back $\dot{H}_p(10)_{Back}$ of the phantom (see **Fig. 2**). Also included in the table are the sum of both detectors $\dot{H}_p(10)_{Total}$ and the contribution of each detector to $\dot{H}_p(10)_{Total}$. When the frontal body part of the phantom is facing the cask, corresponding to an angle of 0°, the main contribution to $\dot{H}_p(10)_{Total}$ comes from the detector at the chest. However, as the angle between phantom and cask increases, the contribution of the detector at the back increases. This phenomenon arrives its maximum when the phantom has an angle 90° with the cask. In this case, the dose rate obtained with each detector represents approximately 50 % of $\dot{H}_p(10)_{Total}$. Hence, the addition of $\dot{H}_p(10)_{Chest}$ and $\dot{H}_p(10)$ is a simple way to account for the angular dependence.

Angle [degrees]	$\dot{H}_p(10)_{Total}$ [µSv/h]	$\dot{H}_p(10)_{Chest}$ [µSv/h]	$\%_{Chest}$ [%]	$\dot{H}_p(10)_{Back}$ [µSv/h]	$\%_{Back}$ [%]
0	1.4	1.2	86	0.19	14
15	1.5	1.3	87	0.20	13
45	1.2	0.97	82	0.22	18
60	1	0.75	75	0.26	25
90	0.89	0.45	50	0.44	50

Tab. 1.
Total $\dot{H}_p(10)$ values and the contribution of the chest and back detectors with different angles between phantom and disposal cask. Calculations were performed in a RSD at 5 meter distance to POLLUX-10 surface.

3.3 Comparison of $\dot{H}_p(10)$ in the rock salt and clay formation drifts during a working scenario

Table 2 shows the calculated dose rate $\dot{H}_p(10)_{Chest}$ and $\dot{H}_p(10)_{Back}$ for the working steps of the disposal scenario shown in **Fig. 4**. $\dot{H}_p(10)_{Total}$ in the table refers to the sum of $\dot{H}_p(10)_{Chest}$ and $\dot{H}_p(10)_{Back}$ while $\%_{Chest}$ and $\%_{Back}$ are their percentage contribution to $\dot{H}_p(10)_{Total}$, respectively. In the table, POLLUX-10 refers to the calculated $\dot{H}_p(10)$ for each working step of the disposal in a RSD, while POLLUX-3 refers to the sum of the calculated $\dot{H}_p(10)$ for two POLLUX-3U and one POLLUX-3M. The calculated dose rate for the disposal of only one POLLUX-3M and one POLLUX-3U is also included in **Tab. 2**.

For the simulated working steps, the angle between phantom and source is always 0°. Hence, the main contribution to $\dot{H}_p(10)_{Total}$ is coming from the chest detector. However, comparing with the results at 0° given in Tab. 1, the contribution of the back dosimeter to $\dot{H}_p(10)_{Total}$ for the worker inside the cabin is higher than that for the worker standing alone in the drift. This effect is attributed to additional backscattered radiation due to the cabin walls and locomotive elements. The calculated dose rate for each working step is similar for POLLUX-3M and for POLLUX-10, while that for POLLUX-3U is 60 % lower that for POLLUX-3M, since no spent MOX fuel was stored in POLLUX-3U. However, to dispose the same amount of waste as in a POLLUX-10, one POLLUX-3M and two POLLUX-3U have to be employed. Therefore, $\dot{H}_p(10)_{Total}$ is 30 % higher for the transport and location in a CLD that in a RSD. For the placement and retreat in CLD the $\dot{H}_p(10)_{Total}$ is more than a 40 % higher than that in the RSD. This reveals that the selection of the host rock can play an important role in the radiation exposure of the workers in such facilities.

The developed methodology can be applied to assess the exposure during the different steps of nuclear waste disposal. In this work the same geometrical parameter were considered for both emplacement drifts. However, due to the lower loading capacity of the cask in CLD, a larger disposal space is required resulting in a larger repository compared to a repository in rock salt *[e.g. DBE-Tec, 2016]*. This leads to a longer transport distance and also longer exposure duration. Since the transport of the

Step	Cask	$\dot{H}_p(10)_{Total}$	$\dot{H}_p(10)_{Chest}$	$\%_{Chest}$	$\dot{H}_p(10)_{Back}$	$\%_{Back}$
Transport	POLLUX-3M	2.8	2.4	87	0.35	13
	POLLUX-3U	0.72	0.63	88	0.09	12
	POLLUX-3	4.2	3.7	88	0.52	12
	POLLUX-10	2.8	2.3	83	0.49	17
Location	POLLUX-3M	2.6	2.2	85	0.38	15
	POLLUX-3U	0.72	0.63	87	0.09	13
	POLLUX-3	4.1	3.5	86	0.57	14
	POLLUX-10	2.6	2.1	80	0.50	20
Placement	POLLUX-3M	0.18	0.15	86	0.02	14
	POLLUX-3U	0.04	0.03	85	0.01	15
	POLLUX-3	0.26	0.22	86	0.04	14
	POLLUX-10	0.19	0.16	82	0.03	18
Retreat	POLLUX-3M	0.07	0.05	73	0.02	27
	POLLUX-3U	0.02	0.01	85	0.002	15
	POLLUX-3	0.10	0.08	77	0.02	23
	POLLUX-10	0.06	0.05	88	0.01	12

Tab. 2.
Total $\dot{H}_p(10)$ values and the contribution of the chest and back detectors for the different disposal steps in RSD and CLD.

cask is one of the steps with the highest personal dose rate, it is plausible to assume that the total personal exposure for disposal in clay formation is higher than for disposal in rock salt.

Since a precise description of the duration of each working step is still unknown, only a dose rate comparison is conducted in this study. The following example will try to demonstrate the importance of this description. Assuming that five hours are required to dispose a POLLUX-10, where four hours are for transport (to simplify, only transport in a drift is considered) and the fifth hour is equally divided amongst the other three steps (20 min/step). For the disposal in CLD the transport of each cask will take longer since the needed space within the drift is larger (assuming 7 h). This will lead to a dose of 12.26 µSv and 30.79 µSv for RSD and CLD, respectively. However as more and more casks are disposed in the drift, the transport time will reduce. Assuming that only 1 h is required for the transport when the drift is almost full, and since the time for the other three steps will be the same, it will lead to a dose of 3.77 µSv and 5.65 µSv for RSD and CLD, respectively.

As illustrated in the example above, the duration of the working steps (especially the transport) plays a decisive role in the personal dose. Therefore, a precise description of the different steps is necessary for a proper comparison between the different disposal options and to provide recommendations for minimizing the occupational radiation exposure.

4 Summary and conclusions

In the current study, the ambient dose equivalent rate $\dot{H}^*(10)$ and the personal dose equivalent rate $\dot{H}_p(10)$ were calculated for emplacement of casks with spent UOX / MOX fuel within two generic deep geological disposal facilities. In the rock salt drift a POLLUX-10 was placed, while for the clay drift with concrete lining a POLLUX-3M and two POLLUX-3U were disposed. In addition, casks free in air were also investigated. Results show that the backscattered radiation of the host rock layers or the concrete lining increases $\dot{H}^*(10)$ in the disposal drift in comparison with a cask FIA. $\dot{H}^*(10)$ for POLLUX-10 in RSD is between 30 % (at the cask surface) and 80 % (at 10 m distance) higher than for POLLUX-10 free in air. For POLLUX-3M and POLLUX-3U, $\dot{H}^*(10)$ in CLD is between 15 and 75 % higher than FIA. The higher increase for POLLUX-10 is caused by the neutron reflection of the rock salt layers, while in the clay drift the presence of oxygen in the concrete lining moderates the neutrons resulting in a lower increase.

For the calculation of $\dot{H}_p(10)$ a mathematical phantom was modelled with two detectors, one at the front side of the chest and another one at the back side. Calculations with different angles between the phantom and the cask show that there is an angular dependence of the registered dose rate values. This effect is enhanced if the dose rate is obtained with only one dosimeter. Therefore, it was proposed to sum up the dose rate obtained with both dosimeters. This methodology was applied to the working scenario for the disposal of a POLLUX® type cask in an emplacement drift. The results of the investigated scenario, where the worker is sitting inside the locomotive cabin and always facing the cask, show that the main contribution to $\dot{H}_p(10)$ comes from the front detector. However, due to the additional neutron scatterings at the cabin, the contribution of the back detector to $\dot{H}_p(10)$ is up to 10 % higher that with the worker just standing alone in the drift. Therefore, a study of the effective dose under this irradiation conditions should be performed to verify if $\dot{H}_p(d)$ is still a conservative assessment.

The calculated personal dose rate for each working step is similar for POLLUX-3M and for POLLUX-10 but is 40 % higher than that for POLLUX-3U. However, to dispose the same amount of waste as in the RSD, three casks have to be placed in the CLD. Therefore each disposal step has to be carried out three times (one POLLUX-3M and two POLLUX-3U, in **Tab. 2** summarized as POLLUX-3), which leads to a higher dose rate (between 35 % and 40 % depending of the working step) for the disposal in CLD. In this study the same geometrical parameter where considered for both galleries. However, due to the lower loading capacity of the cask in CLD, a larger emplacement drift is required.

This leads to a longer transport distance and also longer exposure durations. Since the transport of the canister is one of the steps with the highest personal dose rate, it is plausible to assume that the total personal exposure for disposal in a clay formation drift is higher than for disposal in a rock salt drift.

Acknowledgements

The authors would like to thank our colleagues of DBE TECHNOLOGY GmbH for fruitful discussions regarding the emplacement of POLLUX® casks and for providing a movie showing the working scenario in a drift in rock salt. This study was financially supported by the German Federal Ministry of Education and Research (BMBF; grant number 15S9082E) as part of the joint research project ENTRIA – Disposal Options for Radioactive Residues: Interdisciplinary Analyses and Development of Evaluation Principles.

M. Sc. Héctor Saurí Suárez, winner of the "AMNT 2017 Best Paper Award" during his presentation of the paper "Monte-Carlo Based Comparison of the Personal Dose for Emplacement Scenarios of Spent Nuclear Fuel Casks in Generic Deep Geological Repositories" at the 48th AMNT in Berlin, Germany.

"AMNT 2017 Best Paper Award" ceremony: Dr. Alexander Zulauf, NUKEM Technologies Engineering Services GmbH; Dr. Ralf Güldner, President of DAtF; M. Sc. Héctor Saurí Suárez; Frank Apel, Chairperson of KTG; Dr. Ron Dagan, Karlsruhe Institute of Technology (KIT) (f.l.t.r.)

References

- Bollingerfehr, W., Filbert, W., Lerch, C., & Tholen, M. (2011): *Endlagerkonzepte. Bericht zum Arbeitspaket 5 Vorläufige Sicherheitsanalyse für den Standort Gorleben.* Gesellschaft für Anlagen und Reaktorsicherheit (GRS) mbH. GRS-272.
- BMUB (2015): *National programme for the responsible and safe management of spent fuel and radioactive waste.* Bundesministerium für Umwelt, Naturschutz, Bau und Reaktorsicherheit (BMUB) Berlin, Germany, August 2015.
- Chen, L., Duveau, G., Poutrel, A., Jia, Y., Shao, J.F., & Xie, N. (2014): *Numerical study of the interaction between adjacent galleries in a high-level radioactive waste repository.* International Journal of Rock Mechanics and Mining Sciences Vol. 71, pp. 405–417.
- DBE-Tec (2016): *Flächenbedarf für Endlager für wärmeentwickelnde radioaktive Abfälle:* DBE TECHNOLOGY GmbH, Gutachten für Kommission Lagerung hoch radioaktiver Abfallstoffe, Kommissionsdrucksache K-MAT58
- Filbert, W., Engelmann, H.J., Heda, M., & Neydek, J. (1995): *Direkte Endlagerung ausgedienter Brennelemente (DEAB) – Handhabungsversuche zur Streckenlagerung.* Deutsche Gesellschaft für den Bau und Betrieb von Endlagern für Abfallstoffe mbH (DBE), T60, Peine.
- Filbert, W., Tholen, M., Engelmann, H.J., Graf, R., & Brammer, K.-J. (2011).: *Disposal of Spent Fuel from German Nuclear Power Plants: The Third Option - Disposal of Transport and Storage Casks (Status).* Proceedings of the WM2011 Conference, February 27 - March 3, 2011, Phoenix, USA
- International Commission on Radiological Protection (1991): 1990 *Recommendations of the International Commission on Radiological Protection.* ICRP Publication 60. Ann. ICRP 21 (1-3).
- International Commission on Radiological Protection (1996): *Conversion Coefficients for use in Radiological Protection against External Radiation.* ICRP Publication 74. Ann. ICRP 26 (3-4).
- International Commission on Radiological Protection (2007): *The 2007 Recommendations of the International Commission on Radiological Protection.* ICRP Publication 103. Ann. ICRP 37 (2-4).
- Janberg, K. & Spilker, H. (1998): *Status of the development of final disposal casks and prospects in Germany.* Nuclear Technology, Vol. 121, pp 136-147.
- Leon Vargas, R. Stahlmann, J. & Mintzlaff, V. (2017): *Thermal impact in the geometrical settings in deep geological repositories for HLW with retrievability and monitoring.* Proceedings of the International High-Level Radioactive Waste Management Conference, IHLRWMC2017, April 9 -13, 2017, Charlotte, USA, pp. 664-670.
- Pang, B., Saurí Suárez, H., & Becker, F. (2016): *Individual dosimetry in disposal repository of heat-generating nuclear waste.* Radiation Protection Dosimetry, first published online May 5. 2016
- Peiffer, F., McStocker, B., Gründler, D., Ewig, F., Thomauske, B., Havenith, A., & Kettler, J. (2011): *Abfallspezifikation und Mengengerüst, Basis Ausstieg aus der Kernenergienutzung. Bericht zum Arbeitspaket 3 Vorläufige Sicherheitsanalyse für den Standort Gorleben.* Gesellschaft für Anlagen und Reaktorsicherheit (GRS) mbH. GRS-278.
- Pelowitz, D.B., Goorley, J.T., James, M.R., Booth, T.E., Brown, F.B, Bull, J.S., ... Zukaitis, A. (2013): *MCNP6™ User's Manual Version 1.0.* Los Alamos National Security, LA-CP-13-00634, Rev. 0.
- Siebert, B.R.L., & Schuhmacher, H. (1995): *Quality factors, ambient and personal dose equivalent for neutrons, based on the new ICRU stopping power data for protons and alpha particles.* Radiation Protection Dosimetry, Vol. 58, pp 177-183.
- Stahlmann, J., Mintzlaff, V. & Leon Vargas, R. (2015): *Generische Tiefenlagermodelle mit Option zur Rückholung der radioaktiven Reststoffe: Geologische und Geotechnische Aspekte für die Auslegung. ENTRIA-Arbeitsbericht-03.* TU Braunschweig, Institut für Grundbau und Bodenmechanik, Germany.
- U.S. Department of Energy (data last retrieved July 1. 2016): *Bottle Manikin Absorption (BOMAB) Phantoms.* Retrieved from http://www.id.energy.gov/resl/phantom/bomab.html

Authors

M. Sc. Héctor Saurí Suárez [a]
Dr. Bo Pang [a,b]
Dr. Frank Becker [a]
Dr. Volker Metz [a]

(a) Institute for Nuclear Waste Disposal (INE)
Karlsruhe Institute of Technology (KIT)
Hermann-von-Helmholtz-Platz 1
76344, Eggenstein-Leopoldshafen, Germany

(b) College of Physics and Energy
Shenzhen University
Nanhai Avenue 3688
518060, Nanshan District, Shenzhen, China